IEEE Access
Multidisciplinary | Rapid Review | Open Access Journal

Received December 24, 2020, accepted January 11, 2021, date of publication January 18, 2021, date of current version January 26, 2021.

Digital Object Identifier 10.1109/ACCESS.2021.3052233

A TOA-DOA Hybrid Factor Graph-Based Technique for Multi-Target Geolocation and Tracking

LEI JIANG[1], MENG CHENG[1], (Member, IEEE), AND TAD MATSUMOTO[1,2], (Life Fellow, IEEE)

[1]School of Information Science, Japan Advanced Institute of Science and Technology, Ishikawa 923-1211, Japan
[2]Centre for Wireless Communications, University of Oulu, FI-90014 Oulu, Finland

Corresponding author: Lei Jiang (jianglei12368@jaist.ac.jp)

This work was supported in part by the Hitachi, Ltd., and in part by the Hitachi Kokusai Electric, Inc.

ABSTRACT In this article, we propose a new distributed sensors-based multi-target geolocation and tracking technique. The proposed technique is a joint time-of-arrival (TOA) and direction-of-arrival (DOA) factor graph (FG) for multi-target geolocation (FG-GE), which is further combined with another FG for extend Kalman filtering (FG-GE-EKF) for tracking. Two-dimensional (2D) and three-dimensional (3D) scenarios are considered. In the FG-GE part, a new sensor association technique is proposed to solve the matching problem, which makes the right correspondence between the DOA/TOA information gathered by the distributed sensors and each target. With the proposed sensor association technique, the measured signals from targets can adequately be matched to their corresponding FGs. Thereby, the multi-target geolocation can be reduced to multiple independent single target geolocation. In addition, in the 3D scenario, each target is projected onto three orthogonal planes in the (x, y, z) coordinate. With this operation, the 3D geolocation is decomposed into three 2D geolocation problems. In the FG-GE-EKF part, the whole tracking system can be divided into two steps: prediction step and update step. In the prediction step, the predicted state is obtained from the previous state. Then, we utilize the predicted state as a prior information, and also to update the message exchanged in FG-GE. In the update step, the estimates obtained by FG-GE are regarded as observation state which is used to refine the predicted state, and acquire the current state. With proposed the FG-GE-EKF, the position estimation accuracy and tracking performance can be improved dramatically, without requiring excessively high computational effort.

INDEX TERMS Factor graph (FG), time of arrival (TOA), direction of arrival (DOA), geolocation, extend Kalman filter (EKF), tracking, sensor association.

I. INTRODUCTION

Wireless geolocation is expected to play significant roles in existing and future mobile communication systems, e.g., Enhanced-911 (E-911), smart vehicular communications systems, intelligent navigation [1]–[3], etc. Especially, when the fifth generation (5G) and beyond 5G (B5G) mobile wireless communication systems are considered, accurate geolocation techniques for position-related services are required [4]. For example, when beamforming [5], [6] is applied in 5G systems to eliminate the effects of attenuation in millimeter-wave (mmWave) signaling, target tracking [7] in massive multiple-input multiple-output (MIMO) systems is of significant importance to ensure the effectiveness of beamforming. In recent years, discussions on a variety of indoor geolocation services and their evolution scenarios [8] have been taking place in industry. Reference [9] presents a technique that localizs multiple persons by relying on the reflections of wireless signals reflected from their bodies. A multi-target localization technique based on ML (machine learning) is introduced in [10].

Wireless geolocation is a nonlinear problem and the direct calculation of the multi-target positions is highly complex. To solve the problem, a framework using factor graph (FG) is proposed [11]. FG-based techniques do not require high computational complexity due to the fact that only means

The associate editor coordinating the review of this manuscript and approving it for publication was Liang Hu.

and variances of the messages derived from the measurements, which is assumed to suffer from Gaussian-distributed measurement error, is exchanged between the nodes in the FG [12]. To keep the Gaussianity of the messages exchanged in FG, the first order Taylor series (TS) expansion [13] is applied to approximate the trigonometric functions by linear functions.

In the conventional FG based geolocation systems, different types of information sources such as direction-of-arrival (DOA) [14], time-of-arrival (TOA) [15], time-difference-of-arrival (TDOA) [16] and received-signal-strength (RSS) [17], [18] are used. TDOA-FG, TOA-FG, DOA-FG have been proven to be useful for the detection of single target position. However, FG-based accurate position identification of multiple anonymous targets has yet not been matured. When multiple targets have the same distance to some of the distributed sensors, it is difficult to accurately identify multiple target positions with the TOA/TDOA because the time or difference time of the waves reaching those sensors are almost the same. On the other hand, when multiple targets are located on the same line originating from the some of the sensors, or when the angle difference is small, the DOA detection is unreliable. For the RSS-based technique, off-line training using reference signals from monitoring spots is required beforehand, which can not be obtained from multiple anonymous targets case.

The background described above has motivated this contribution. In this article, a new joint TOA-DOA technique is proposed not only to compensate each technique's shortcomings but also to solve the problem of associating the observation and targets.

To perform tracking, the extended Kalman filter (EKF) is used in this article, as in [15], [19]. The target positions estimated by FG-GE can be regarded as observation state in the tracking process. However, the variance of the observation error can not be directly detected. Instead, the smallest variance of the observation which can be determined by the Cramér–Rao lower bound (CRLB) is used as the variance of the observation error [19], [20]. The proposed algorithm that combines FGs for GE and EKF is referred to as FG-GE-EKF for the notation convenience. The moving targets can be localized by the proposed FG-GE and FG-GE-EKF. The output of FG-GE is used as observation state, to refine the predicted state which can be obtained from the prior state in FG-GE-EKF. The proposed algorithm combines all those core functionalities, sensor association, geolocation and tracking, and hence it works dynamically.

This article investigates distributed sensors-based geolocation technique.[1] The main contributions of this article are summarized as follows.

1) First of all, a new two-dimension (2D) joint TOA-DOA based FG is proposed for multi-target geolocation and tracking by integrating the EKF algorithm into the FG. Furthermore, the proposed technique is then extended to a three-dimension (3D) scenario.
2) A new sensor association algorithm based on the joint TOA-DOA measurements is proposed to solve the target-observation matching problem occurring typically in the distributed sensors systems in 2D and 3D scenarios.
3) A switching algorithm for the use of either TOA or DOA is proposed to alleviate the shortcomings inherent in TOA-only and DOA-only algorithms described before.

This article is organized as follows. The geolocation and tracking models are described in Section II. In Section III, the proposed sensor association algorithm, combined with the joint FG-GE and FG-GE-EKF are introduced both in 2D and 3D scenarios. The performance of the proposed FG-GE and FG-GE-EKF algorithms are evaluated by a series of simulations, and the results presented in Section IV. Finally, the conclusion of this contribution is provided in Section V.

II. SYSTEM MODEL

We start with a 2D scenario having N distributed sensors located at (X_n, Y_n), $n = \{1, 2, \ldots, N\}$, in the global coordinate, of which location are assumed to be known to the fusion center. I anonymous multiple targets are located at $(x_{i,k}, y_{i,k})$, where $i = \{1, 2, \ldots, I\}$ and $k = \{1, 2, \ldots, K\}$ are the target and timing indexes, respectively.

For the simplicity, the target index i is omitted unless required. The measurement of DOA at the timing k is given by

$$\widehat{\varphi}_n = h(\varphi_{n,k}) + u_{\varphi,n,k} \tag{1}$$

with the measurement error $u_{\varphi,n,k} \sim \mathcal{N}(0, \sigma_\varphi^2)$ and $h(\varphi_{n,k})$ the true DOA, given by

$$h(\varphi_{n,k}) = \arctan\left(\frac{Y_n - y_k}{X_n - x_k}\right) \tag{2}$$

The measurement of TOA at the timing k is converted to the Euclidean distance by

$$\widehat{d}_{2D,n} = c \cdot \bigtriangleup t = q(d_{2D,n,k}) + v_{2D,n,k} \tag{3}$$

with the measurement error $v_{2D,n,k} \sim \mathcal{N}(0, \sigma_d^2)$, c the light speed, $\bigtriangleup t$ the time difference between the transmit and receive timings and $q(d_{2D,n,k})$ the true TOA, given by

$$q(d_{2D,n,k}) = \sqrt{(X_n - x_k)^2 + (Y_n - y_k)^2} \tag{4}$$

In this article, we assume that the sensors and targets share the same time reference, such as in aviation control or commercial navigation systems.

In the 3D scenario, φ_n is the same measurement as in the X-Y plane expressed by (1). Another measurement of

[1] It should be noted that each sensor can identify the number of the targets by using some information theoretic criterion, such as Akaike criterion or MDL criterion. The results are sent to the fusion center. Hence, number of targets is known to the fusion center by receiving the measurement data from the targets.

DOA [21] is the elevation angle given by

$$\widehat{\theta}_n = \arctan\left(\frac{\sqrt{(Y_n - y_k)^2 + (X_n - x_k)^2}}{Z_n - z_k}\right) + u_{\theta,n,k} \quad (5)$$

at timing k, with $u_{\theta,n,k} \sim \mathcal{N}(0, \sigma_\theta^2)$ the measurement error. The measurement of TOA in the 3D scenario is given by

$$\widehat{d}_{3D,n} = \sqrt{(X_n - x_k)^2 + (Y_n - y_k)^2 + (Z_n - z_k)^2} + v_{3D,n,k} \quad (6)$$

with $v_{3D,n,k} \sim \mathcal{N}(0, \sigma_d^2)$ the measurement error.

For the tracking system, the multi-target non-linear discrete state-space model (SSM) is used, as in [19]. I anonymous target positions are located in $s_k = [x_k, y_k]^T$ or $s_k = [x_k, y_k, z_k]^T$ at timing k in the 2D and 3D scenarios, respectively. The SSM equation is given by

$$s_k = f(s_{k-1}) + w_k, \quad (7)$$

where $f(\cdot)$ is a non-linear function, and $w_k = [w_{x,k}, w_{y,k}]^T$ or $w_k = [w_{x,k}, w_{y,k}, w_{z,k}]^T$ the white Gaussian noise vector in the 2D and 3D scenarios, respectively. In order to keep the Gaussianity of the messages in the FG, the first order Taylor series (TS) expansion needs to be used to approximate $f(\cdot)$ by a linear function. The first order TS is given by

$$f(s_{k-1}) \approx f(\alpha) + f'(\alpha)(s_{k-1} - \alpha), \quad (8)$$

where α is the center point of the TS expansion, $f(\alpha)$ is the current position s_{k-1}, and the first order derivative $f'(\alpha)(s_{k-1} - \alpha) = v_{k-1} \cdot \triangle t$ is the distance between s_{k-1} and s_k without loss of generality, we normalize $\triangle t = 1$. Then, (7) can be rewritten as

$$s_k \approx s_{k-1} + v_{k-1} + w_k. \quad (9)$$

The velocity v_{k-1} is updated by EKF. The observation state j_k is given by

$$j_k = g(s_k) + e_k \quad (10)$$

with $e_k \sim \mathcal{N}(0, \sigma_e^2)$ the observation noise. Since e_k is unknown, we use the variance of φ_k that achieves the smallest σ_e^2, which can be calculated from the CRLB [19].

III. PROPOSED ALGORITHM

In this section, the proposed algorithm for 2D is detailed, including multi-target position detection and tracking, and its extension to the 3D scenario.

A. POSITION DETECTION

It should be noted that all the targets are anonymous. The matching problem between distributed sensors' observations and multiple anonymous targets is focused on in this subsection. To recognize the targets, a simple, yet useful algorithm is proposed.

1) SENSOR ASSOCIATION

In the 2D scenario, $(\varphi_{i,n}, d_{i,n})$ is the *i-th* set of DOA and TOA measurement from target i to the sensor n, where $i = \{1, 2, \cdots, I\}$ ans $n = \{1, 2, \cdots, N\}$, as shown in Fig. 1(a). By using trigonometry method, the rough estimate of the position can be calculated by

$$\begin{bmatrix} \hat{x}_{n,i} \\ \hat{y}_{n,i} \end{bmatrix} = \begin{bmatrix} d_{n,i} \times \cos\varphi_{n,i} \pm X_n \\ d_{n,i} \times \sin\varphi_{n,i} \pm Y_n \end{bmatrix}. \quad (11)$$

Let sensor n obtain L sets of DOA and TOA measurement from the target i. Each set of measurements is used to calculate the location information. Therefore, for sensor n, I clusters of targets are obtained. However, the position estimates obtained by (11) are unreliable because the estimation of $\widehat{x}$ and $\widehat{y}$ uses TOA and DOA observed by each sensor without message change over the FG. As shown in Fig. 1(b), the positions of the targets in each cluster are largely scattered.

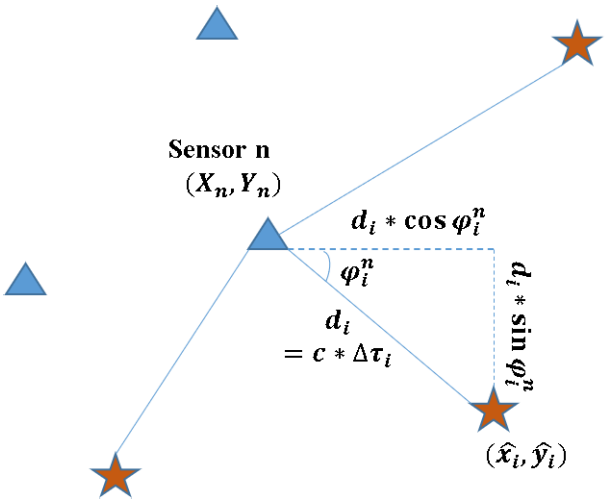

(a) 2D scenario

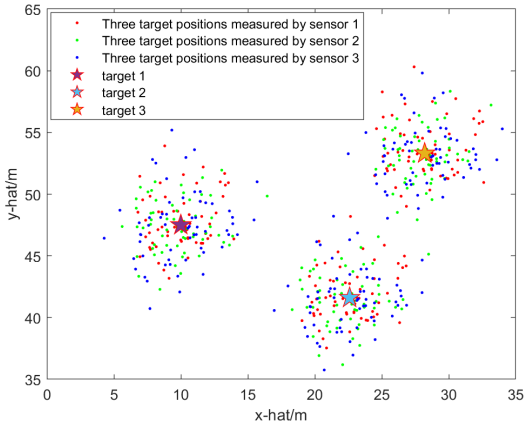

(b) Rough estimates of targets in 2D scenario

FIGURE 1. Proposed sensor association algorithm in 2D scenario.

In the 3D scenario, the rough estimates of the positions can be calculated by

$$\begin{bmatrix} \hat{x}_{n,i} \\ \hat{y}_{n,i} \\ \hat{z}_{n,i} \end{bmatrix} = \begin{bmatrix} d_{n,i} \times \sin\theta_{n,i} \times \cos\varphi_{n,i} \pm X_n \\ d_{n,i} \times \cos\theta_{n,i} \times \sin\varphi_{n,i} \pm Y_n \\ d_{n,i} \times \cos\theta_{n,i} \pm Z_n \end{bmatrix}. \quad (12)$$

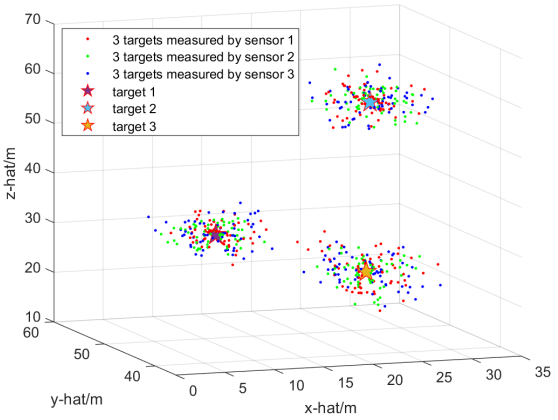

FIGURE 2. Rough estimates of targets in 3D scenario.

As shown in Fig.2, the positions in each cluster are also largely scattered because of the same reason as in the 2D case. Even though the initial position detection without using FG iteration is rough and the positions are scattered, we can identify from which cluster the observations are. This information makes it possible to make the target-observation matching, and hence the measurement data can be properly input to the corresponding FG.

2) DOA-TOA SWITCHING ALGORITHM

In this sub-section, the problem of positioning in certain critical situations is discussed. There may exist some sensors from which multiple targets have the same distance to such sensors. In this case, TOA cannot identify the positions accurately because the arriving timings of the waves from the targets at such sensor are very close. On the other hand, there may exist some sensors when the multiple targets are on the same line originating from those sensors, or the angle differences are small, DOA detection is unreliable. Thus, a simple technique is proposed, which switches the use of either DOA or TOA. Assume that n-th sensor can obtain three measurement of DOA with mean and variance $(\varphi_{n,1}, \sigma_\varphi^2)$, $(\varphi_{n,2}, \sigma_\varphi^2)$ and $(\varphi_{n,3}, \sigma_\varphi^2)$. Calculate the relative angles by subtracting each of the two angles, and set the angle interval $[-k\sigma_\varphi, k\sigma_\varphi]$, where k is determined empirically. In this article, we set $k = 2$ to identify weather or not the measured DOAs are reliable. For the n-th sensor, TOA is used instead of DOA if one or some of the relative angles is/are within this interval. The pseudo code of proposed algorithm is shown in Algorithm 1, as below.

Algorithm 1 Switching Algorithm

Initialization: φ_1, φ_2. φ_3 are the DOA measurement from target 1,2,3 to n-th sensor; 1: $\bigtriangleup\varphi_1 = \varphi_1 - \varphi_2$;
2: $\bigtriangleup\varphi_2 = \varphi_2 - \varphi_3$;
3: $\bigtriangleup\varphi_3 = \varphi_3 - \varphi_1$;
4: **if** $\bigtriangleup\varphi_1 \cup \bigtriangleup\varphi_2 \cup \bigtriangleup\varphi_3 \in [-k\sigma_\varphi, k\sigma_\varphi]$ **then**
5: Apply to TOA
6: else
7: Apply to DOA

3) FG-GE

The proposed joint DOA-TOA based FG is provided in this sub-section. In order to preserve the Gaussianity of the FG messages, the first order TS expansion centered at the point β, is used to approximate the true DOA and TOA information, expressed by (2) and (4), by linear functions, as

$$\varphi_k \approx h(\beta) + \frac{\partial h(\varphi_k)}{\partial x_k}(x_k - \beta_x) + \frac{\partial h(\varphi_k)}{\partial y_k}(y_k - \beta_y) \quad (13)$$

and

$$d_{2D,k} \approx q(\beta) + \frac{\partial q(d_{2D,k})}{\partial x_k}(x_k - \beta_x) + \frac{\partial q(d_{2D,k})}{\partial y_k}(y_k - \beta_y) \quad (14)$$

with $\beta = [\beta_x, \beta_y]^T$. To achieve simple, yet accurate approximation, let β be equal to predicted state $s_{k|k-1}$, which is determined by the previous state. The target index i and the sensor index n are omitted. Then, φ_k can be approximated as

$$\varphi_k \approx \lambda_1 x + \lambda_2 y + \lambda_3, \quad (15)$$

where λ_1, λ_2 and λ_3 are the constants, given by

$$\lambda_1 = \frac{Y - y_{k|k-1}}{(X - x_{k|k-1})^2 + (Y - y_{k|k-1})^2}, \quad (16)$$

$$\lambda_2 = \frac{-(X - x_{k|k-1})}{(X - x_{k|k-1})^2 + (Y - y_{k|k-1})^2}, \quad (17)$$

$$\lambda_3 = \frac{(X - x_{k|k-1})y_{k|k-1} - (Y - y_{k|k-1})x_{k|k-1}}{(X - x_{k|k-1})^2 + (Y - y_{k|k-1})^2} + \arctan\left(\frac{Y - y_{k|k-1}}{X - x_{k|k-1}}\right). \quad (18)$$

The target position can then be derived as:

$$x = \frac{\varphi_k - \lambda_2 y - \lambda_3}{\lambda_1}, \quad (19)$$

$$y = \frac{\varphi_k - \lambda_1 x - \lambda_3}{\lambda_2}. \quad (20)$$

In the same way as in DOA, true TOA d_k can be approximated as

$$d_k = \tau_1 x + \tau_2 y + \tau_3, \quad (21)$$

where τ_1, τ_2 and τ_3 are the constants, given by

$$\tau_1 = \frac{-(X - x_{k|k-1})}{\sqrt{(X - x_{k|k-1})^2 + (Y - y_{k|k-1})^2}}, \quad (22)$$

$$\tau_2 = \frac{-(Y - y_{k|k-1})}{\sqrt{(X - x_{k|k-1})^2 + (Y - y_{k|k-1})^2}}, \quad (23)$$

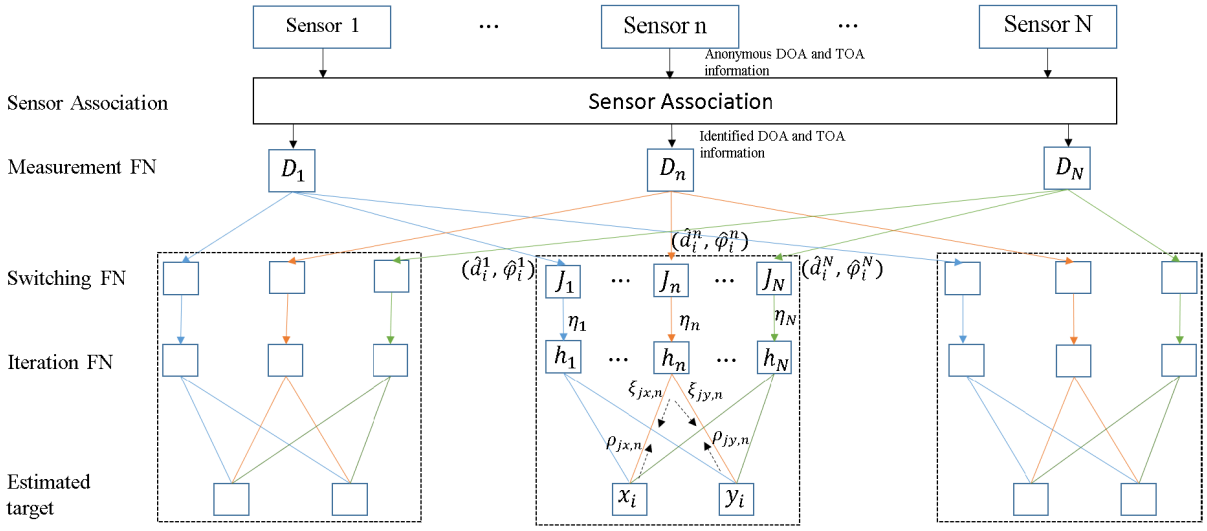

FIGURE 3. Proposed FG-GE in 2D scenario.

$$\tau_3 = \frac{(Y - y_{k|k-1})y_{k|k-1} + (X - x_{k|k-1})x_{k|k-1}}{\sqrt{(X - x_{k|k-1})^2 + (Y - y_{k|k-1})^2}} + \sqrt{(X - x_{k|k-1})^2 + (Y - y_{k|k-1})^2}. \tag{24}$$

Therefore, the target position can be derived by

$$x = \frac{d_k - \tau_2 y - \tau_3}{\tau_1}, \tag{25}$$

$$y = \frac{d_k - \tau_1 x - \tau_3}{\tau_2}. \tag{26}$$

The FG for the position detection is illustrated in Fig. 3. It should be noted that the each component FG in one box with dotted line described in Fig. 3 is used to estimate the position of one target. The positions of the rest of the targets can be obtained in the same way. After the sensor association process, the measured DOA and TOA messages are calculated by the measurement function node (FN) D_n. The calculated mean and variance, i.e., $(m_{\varphi,n}, \sigma^2_{\varphi,n})$ and $(m_{d,n}, \sigma^2_{d,n})$, are passed through DOA-TOA switching FN C_n. In this node, either DOA or TOA message is selected, according to Algorithm 1, and is sent to the iteration FN. Let η_n denote the DOA or TOA message from the DOA-TOA switching FN. Let $\xi_{j_{x,n}}$ and $\xi_{j_{y,n}}$ denote downward messages from the iteration FN h_n to the estimated target FN J_x and J_y, respectively. Then, $\rho_{j_{x,n}}$ and $\rho_{j_{y,n}}$ are the upward messages from J_x and J_y to h_n, respectively. If the DOA measurement is selected by node C_n, η_n denotes the DOA message, i.e., $(m_{\varphi,n}, \sigma^2_{\varphi,n})$. Otherwise, $(m_{d,n}, \sigma^2_{d,n})$ denotes the mean and the variance of the TOA message. According to (16)-(20), the iteration process is described as follows.

- Update of downward messages:

$$m_{\xi_{j_{x,n}}} = \frac{1}{\lambda_{1,n}} m_{\eta_n} - \frac{\lambda_{2,n}}{\lambda_{1,n}} m_{\rho_{j_{y,n}}} - \frac{\lambda_{3,n}}{\lambda_{1,n}}, \tag{27}$$

$$\sigma^2_{\xi_{j_{x,n}}} = \frac{1}{\lambda^2_{1,n}} \sigma^2_{\eta_n} + \left(\frac{\lambda_{2,n}}{\lambda_{1,n}}\right)^2 \sigma^2_{\rho_{j_{y,n}}}, \tag{28}$$

$$m_{\xi_{j_{y,n}}} = \frac{1}{\lambda_{2,n}} m_{\eta_n} - \frac{\lambda_{1,n}}{\lambda_{2,n}} m_{\rho_{j_{x,n}}} - \frac{\lambda_{3,n}}{\lambda_{2,n}}, \tag{29}$$

$$\sigma^2_{\xi_{j_{y,n}}} = \frac{1}{\lambda^2_{2,n}} \sigma^2_{\eta_n} + \left(\frac{\lambda_{1,n}}{\lambda_{2,n}}\right)^2 \sigma^2_{\rho_{j_{x,n}}}. \tag{30}$$

If the TOA measurement is selected by the node C_n, η_n denotes the TOA message, i.e., $(m_{d,n}, \sigma^2_{d,n})$, where only the constants λ_1, λ_2 and λ_3 are replaced by the constants τ_1, τ_2 and τ_3 according to (22)-(26).

- Update of upward messages:

$$\frac{1}{\sigma^2_{\rho_{j_{x,n}}}} = \sum_{i=1, i\neq n}^{N} \frac{1}{\sigma^2_{\xi_{j_{x,i}}}}, \tag{31}$$

$$m_{\rho_{j_{x,n}}} = \sigma^2_{\rho_{j_{x,n}}} \cdot \sum_{i=1, i\neq n}^{N} \frac{m_{\xi_{j_{x,i}}}}{\sigma^2_{\xi_{j_{x,i}}}}, \tag{32}$$

$$\frac{1}{\sigma^2_{\rho_{j_{y,n}}}} = \sum_{i=1, i\neq n}^{N} \frac{1}{\sigma^2_{\xi_{j_{y,i}}}}, \tag{33}$$

and

$$m_{\rho_{j_{y,n}}} = \sigma^2_{\rho_{j_{y,n}}} \cdot \sum_{i=1, i\neq n}^{N} \frac{m_{\xi_{j_{y,i}}}}{\sigma^2_{\xi_{j_{y,i}}}}. \tag{34}$$

The iteration is performed until convergence or until the maximum iteration time is reached. Finally, the estimated position is obtained by (m_{j_x}, m_{j_y}), which can be given by

$$\frac{1}{\sigma^2_{j_x}} = \sum_{i=1}^{N} \frac{1}{\sigma^2_{\xi_{j_{x,i}}}}, \tag{35}$$

$$\frac{1}{\sigma_{j_y}^2} = \sum_{i=1}^{N} \frac{1}{\sigma_{\xi_{j_y,i}}^2}, \tag{36}$$

$$m_{j_x} = \sigma_{j_x}^2 \cdot \sum_{i=1}^{N} \frac{m_{\xi_{j_x,i}}}{\sigma_{\xi_{j_x,i}}^2}, \tag{37}$$

and

$$m_{j_y} = \sigma_{j_y}^2 \cdot \sum_{i=1}^{N} \frac{m_{\xi_{j_y,i}}}{\sigma_{\xi_{j_y,i}}^2}. \tag{38}$$

Note that (m_{j_x}, m_{j_y}) can be used as the observation state in EKF. However, according to (10), the variance $(\sigma_{j_x}^2, \sigma_{j_y}^2)$ is not equal to the variance of e_k, of which the smallest value is calculated by the CRLB [19], as shown in Appendix, and is used as representing $(\sigma_{j_x}^2, \sigma_{j_y}^2)$.

B. MULTI-TARGET TRACKING

A multi-target tracking is based on EKF presented in [19]. For the completeness of this article, the EKF algorithm is described in Appendix.

C. 3D GEOLOCATION AND TRACKING

In this sub-section, the proposed geolocation and tracking technique in the 3D scenario is described. As in the 2D's case, it is also composed of the two steps: 3D position detection by FG-GE, and 3D tracking by FG-GE-EKF. Since the 3D tracking technique is exactly the same as the 2D, only 3D multi-target position detection is investigated.

In the 3D scenario, since the situation where the multiple targets are on the same line originating from a sensor rarely exists, the DOA-TOA switching algorithm is omitted. This sub-section proposes a technique for estimating the multi-target positions, which can be performed using three projected 2D FGs.

1) PROJECTION ONTO 2D PLANES

First of all, we project the target onto the Y-Z and X-Z planes as shown in Fig.4. To combine the three projected 2D FGs for identifying target position, we need the angle information on the projected plane between the projected point and each sensor. Assume that sensors can measure the azimuth angle φ, the elevation angle θ and the relative distance d based on (1), (5) and (6). The relative distance in the (X, Y, Z) coordinate can be calculated as

$$\begin{bmatrix} \triangle x \\ \triangle y \\ \triangle z \end{bmatrix} = \begin{bmatrix} d \times \sin\theta \times \cos\varphi \\ d \times \cos\theta \times \sin\varphi \\ d \times \cos\theta \end{bmatrix}. \tag{39}$$

The tangent of the angle υ between the projected point (x, z) and the sensor is given by

$$\tan\upsilon = \frac{\triangle x}{\triangle z} = \tan\theta \cdot \cos\varphi. \tag{40}$$

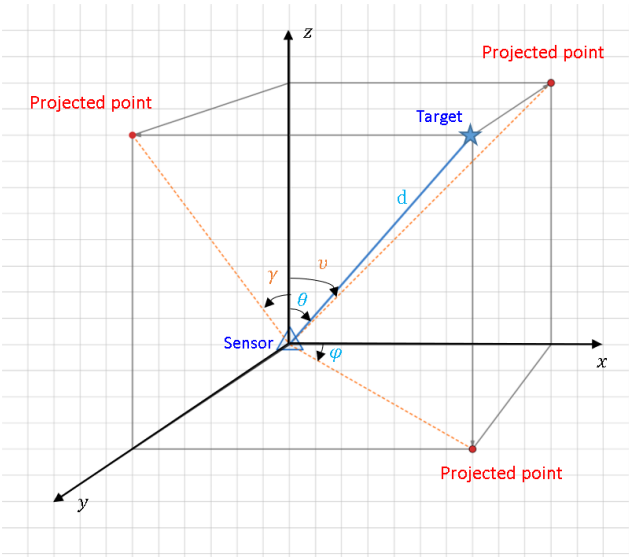

FIGURE 4. Projection onto 2D planes.

The tangent of the angle γ between the projection point (y, z) and the sensor is given by

$$\tan\gamma = \frac{\triangle y}{\triangle z} = \tan\theta \cdot \sin\varphi. \tag{41}$$

The mean and the variance of the product of two independent Gaussian random variables, $a \sim \mathcal{N}(m_a, \sigma_a^2)$ and $b \sim \mathcal{N}(m_b, \sigma_b^2)$, can be given by

$$m_{a\cdot b} = m_a \cdot m_b, \tag{42}$$

$$\sigma_{a\cdot b}^2 = m_a^2 \cdot \sigma_b^2 + m_b^2 \cdot \sigma_a^2 + \sigma_a^2 \cdot \sigma_b^2, \tag{43}$$

where $a, b \in \{\tan\theta, \cos\varphi, \sin\varphi\}$. It should be noted that (40) and (41) are nonlinear function which does not allow us to use the Gaussian assumption of the messages in FG. Therefore, the first-order TS expansion is applied to approximate the trigonometric functions as,

$$f(\alpha) \approx f(m_\alpha) + f'(m_\alpha)(\alpha - m_\alpha), \tag{44}$$

where $f(\alpha)$ is either $\tan\theta$, $\cos\varphi$ or $\sin\varphi$, and $f(m_\alpha)$ is either $\tan(m_\theta)$, $\cos(m_\varphi)$ or $\sin(m_\varphi)$. Then, the mean and the variance $(m_{f(\alpha)}, \sigma_{f(\alpha)}^2)$ can be given by

$$m_{f(\alpha)} \approx f(m_\alpha), \tag{45}$$

$$\sigma_{f(\alpha)}^2 \approx [f'(m_\alpha)]^2 \cdot \sigma_\alpha^2. \tag{46}$$

The mean and the variance of the trigonometric function calculated from (45) and (46) are summarized in TABLE 1.

With the approximation described above, the tangent of the angle υ can further be expressed as

$$m_{\tan(\upsilon)} = m_{\tan(\theta)} \cdot m_{\cos(\varphi)}, \tag{47}$$

$$\sigma_{\tan(\upsilon)}^2 = m_{\tan(\theta)}^2 \sigma_{\sin(\varphi)}^2 + m_{\sin(\varphi)}^2 \sigma_{\tan(\theta)}^2 + \sigma_{\tan(\theta)}^2 \sigma_{\sin(\varphi)}^2. \tag{48}$$

Again, by using (45) and (46), the mean and the variance of υ can be obtained by

$$m_\upsilon \approx \arctan(m_{\tan(\upsilon)}), \tag{49}$$

TABLE 1. Approximated means and variances of related trigonometric functions.

	Approximated mean	Approximated variance
$\tan(\alpha)$	$\tan(m_\alpha)$	$\sec^4(m_\alpha)\cdot\sigma_\alpha^2$
$\sin(\alpha)$	$\sin(m_\alpha)$	$\cos^2(m_\alpha)\cdot\sigma_\alpha^2$
$\cos(\alpha)$	$\cos(m_\alpha)$	$\sin^2(m_\alpha)\cdot\sigma_\alpha^2$

$$\sigma_\upsilon^2 \approx \frac{\sigma_{\tan(\upsilon)}^2}{\sec^4(m_\upsilon)}. \tag{50}$$

The mean and the variance of angle γ can also be calculated in the same way.

2) FG-GE

In the same way as the proposed FG algorithm in the 2D scenario was derived, we apply the first-order TS expansion to approximate the true DOA φ_k, υ_k and γ_k at the timing k. Since φ_k has been discussed in the 2D scenario, only υ_k and γ_k are discussed in this sub-section. Note that the true DOA υ_k and γ_k are given by

$$\upsilon_k = \arctan\left(\frac{X - x_{\upsilon,k}}{Z - z_{\upsilon,k}}\right), \tag{51}$$

$$\gamma_k = \arctan\left(\frac{Y - y_{\upsilon,k}}{Z - z_{\upsilon,k}}\right). \tag{52}$$

By using the first-order TS expansion to approximate (51), centered at the point $s_{\upsilon,k|k-1}$, υ_k can further be expressed as

$$\upsilon_k \approx a_1 x_{\upsilon,k} + a_2 z_{\upsilon,k} + a_3, \tag{53}$$

where

$$a_1 = \frac{-(Z - z_{\upsilon,k|k-1})}{(Z - z_{\upsilon,k|k-1})^2 + (X - x_{\upsilon,k|k-1})^2}, \tag{54}$$

$$a_2 = \frac{X - x_{\upsilon,k|k-1}}{(Z - z_{\upsilon,k|k-1})^2 + (X - x_{\upsilon,k|k-1})^2}, \tag{55}$$

$$a_3 = \frac{(Z - z_{\upsilon,k|k-1})x_{\upsilon,k|k-1} - (X - x_{\upsilon,k|k-1})z_{\upsilon,k|k-1}}{(Z - z_{\upsilon,k|k-1})^2 + (X - x_{\upsilon,k|k-1})^2} + \arctan\left(\frac{X - x_{\upsilon,k|k-1}}{Z - z_{\upsilon,k|k-1}}\right). \tag{56}$$

Therefore, the target position can be expressed as

$$x_{\upsilon,k} = \frac{\upsilon_k - a_2 z_{\upsilon,k} - a_3}{a_1}, \tag{57}$$

$$z_{\upsilon,k} = \frac{\upsilon_k - a_1 x_{\upsilon,k} - a_3}{a_2}. \tag{58}$$

Similarly, γ_k can be expressed as

$$\gamma_k \approx b_1 y_{\gamma,k} + b_2 z_{\gamma,k} + b_3, \tag{59}$$

where

$$b_1 = \frac{-(Z - z_{\gamma,k|k-1})}{(Z - z_{\gamma,k|k-1})^2 + (Y - y_{\gamma,k|k-1})^2}, \tag{60}$$

$$b_2 = \frac{Y - y_{\gamma,k|k-1}}{(Z - z_{\gamma,k|k-1})^2 + (Y - y_{\gamma,k|k-1})^2}, \tag{61}$$

$$b_3 = \frac{(Z - z_{\gamma,k|k-1})y_{\gamma,k|k-1} - (Y - y_{\gamma,k|k-1})z_{\gamma,k|k-1}}{(Z - z_{\gamma,k|k-1})^2 + (Y - y_{\gamma,k|k-1})^2} + \arctan\left(\frac{Y - y_{\gamma,k|k-1}}{Z - z_{\gamma,k|k-1}}\right). \tag{62}$$

The target position can then be expressed by

$$y_{\gamma,k} = \frac{\gamma_k - b_2 z_{\gamma,k} - b_3}{b_1}, \tag{63}$$

$$z_{\gamma,k} = \frac{\gamma_k - b_1 y_{\gamma,k} - b_3}{b_2}. \tag{64}$$

According to (16)-(20) and (51)-(64), the FG-GE in 3D (3D FG-GE) using the three projected planes is illustrated in Fig.5. A new function node, combination function node, is introduced between iteration function node and estimated target function node. In the combination function node, the fact that the product of two independent Gaussian PDFs, following $\mathcal{N}(m_a, \sigma_a^2)$ and $\mathcal{N}(m_b, \sigma_b^2)$, becomes also Gaussian PDF with $\mathcal{N}\left(\frac{m_a\sigma_b^2 + m_b\sigma_a^2}{\sigma_a^2+\sigma_b^2}, \frac{1}{\frac{1}{\sigma_a^2}+\frac{1}{\sigma_b^2}}\right)$ is used. Therefore, the means and the variances of the message for the combination function node can be calculated by

$$m_{j_x} = \frac{m_{\xi_{jx,\varphi}}\cdot\sigma_{\xi_{jx,\upsilon}}^2 + m_{\xi_{jx,\upsilon}}\cdot\sigma_{\xi_{jx,\varphi}}^2}{\sigma_{\xi_{jx,\varphi}}^2 + \sigma_{\xi_{jx,\upsilon}}^2}, \tag{65}$$

$$m_{j_y} = \frac{m_{\xi_{jy,\varphi}}\cdot\sigma_{\xi_{jy,\gamma}}^2 + m_{\xi_{jy,\gamma}}\cdot\sigma_{\xi_{jy,\varphi}}^2}{\sigma_{\xi_{jy,\varphi}}^2 + \sigma_{\xi_{jy,\gamma}}^2}, \tag{66}$$

$$m_{j_z} = \frac{m_{\xi_{jz,\upsilon}}\cdot\sigma_{\xi_{jz,\gamma}}^2 + m_{\xi_{jz,\gamma}}\cdot\sigma_{\xi_{jz,\upsilon}}^2}{\sigma_{\xi_{jz,\upsilon}}^2 + \sigma_{\xi_{jz,\gamma}}^2}, \tag{67}$$

and

$$\sigma_{j_x}^2 = \frac{1}{\frac{1}{\sigma_{\xi_{jx,\varphi}}^2} + \frac{1}{\sigma_{\xi_{jx,\upsilon}}^2}}, \tag{68}$$

$$\sigma_{j_y}^2 = \frac{1}{\frac{1}{\sigma_{\xi_{jy,\varphi}}^2} + \frac{1}{\sigma_{\xi_{jy,\gamma}}^2}}, \tag{69}$$

$$\sigma_{j_z}^2 = \frac{1}{\frac{1}{\sigma_{\xi_{jz,\upsilon}}^2} + \frac{1}{\sigma_{\xi_{jz,\gamma}}^2}}. \tag{70}$$

It also should be noted that $\sigma_z^2 = \left[\sigma_{j_x}^2, \sigma_{j_y}^2, \sigma_{j_z}^2\right]^T$ is replaced by the smallest value of σ_e^2, obtained by the CRLB [19], as in the 2D's case.

IV. SIMULATIONS

A. 2D SCENARIO

In this sub-section, results of a series of simulations conducted to evaluate the proposed FG-GE and FG-GE-EKF algorithms in the 2D, three targets scenario are presented. The process equations used in the simulation for the three target case are shown as below:

$$x_{1,k} = x_{1,k-1} + \cos\left(\frac{x_{1,k-1}\Phi}{k}\right) + \omega_{x,k}, \tag{71}$$

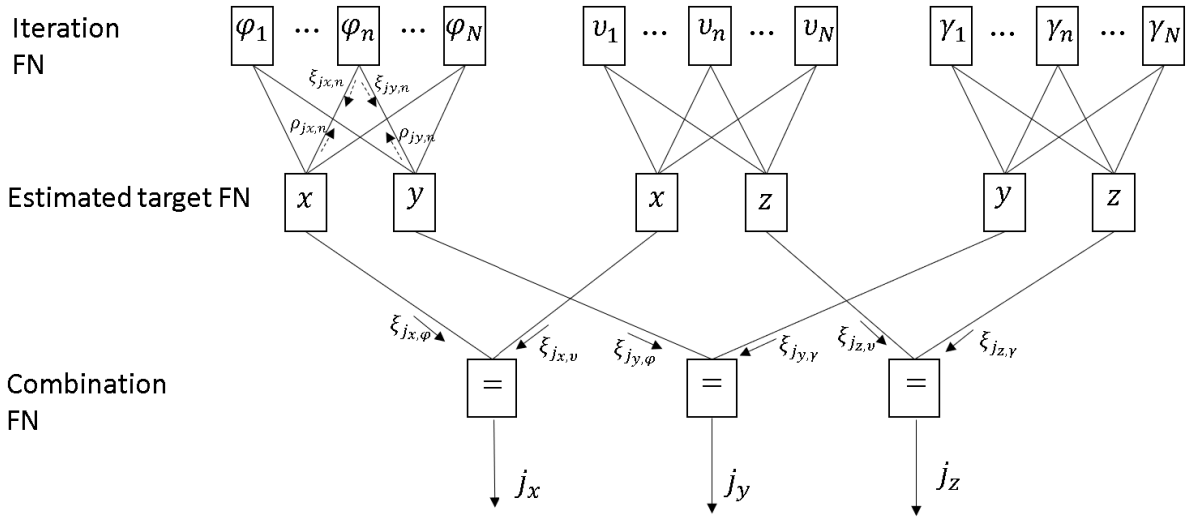

FIGURE 5. Proposed FG-GE in 3D scenario.

$$y_{1,k} = y_{1,k-1} + \sin\left(\frac{x_{1,k-1}\Phi}{k}\right) + \omega_{y,k}, \quad (72)$$

$$x_{2,k} = x_{2,k-1} + \cos(0.2k\Phi) + \omega_{x,k}, \quad (73)$$

$$y_{2,k} = y_{2,k-1} + \sin(0.2k\Phi) + \omega_{y,k}, \quad (74)$$

$$x_{3,k} = x_{3,k-1} + (0.02k - 0.074) + \omega_{x,k}, \quad (75)$$

$$y_{3,k} = y_{3,k-1} + (0.03k - 0.074) + \omega_{y,k}, \quad (76)$$

where Φ was set at $\pi/10$ and the timing $k = \{1, 2, \cdots, 40\}$. The initial points of three targets were set at (10, 47.5), (22.6, 41.6) and (28.2, 53.3). Three sensors were located at (-20, -10), (45, 110) and (100, 30). In the 2D geolocation, number of the sensors needed to identify the positions of the targets is common, regardless of how many targets exist. This is because the sensor association makes FGs for each target independent. As shown in Fig. 3, at least three sensors are need to exchange the messages in each FG. According to the assumptions discussed before, the measured DOAs and TOAs suffer from wihte Gaussian error. At each timing, sensors obtain 60 DOA and TOA samples having standard deviation $\sigma_\varphi = 3°$ and $\sigma_d = 15$ (meter), respectively. Let the maximum iteration time $J = 10$ and $\sigma_\omega^2 = 0.05$. The convergence behavior is shown in Fig.6, with the initial guess was set at (0, 0). It can be found that even the initial guess is very far away form the 3 targets, with 7 or 8 iterations, they converge into the points very close to the true targets positions.

In the simulation, the proposed algorithm which performs the joint DOA-TOA algorithm, was compared with the algorithm using DOA-only and TOA-only in FG-GE. The estimated positions of the three targets using FG-GE, as well as the tracking trajectories using FG-GE-EKF are shown in Fig.7. Clearly, it can be observed that the proposed joint DOA-TOA algorithm can achieve the highest accuracy in tracking and target acquisition. The co-located targets can also be estimated based on the each previous state from

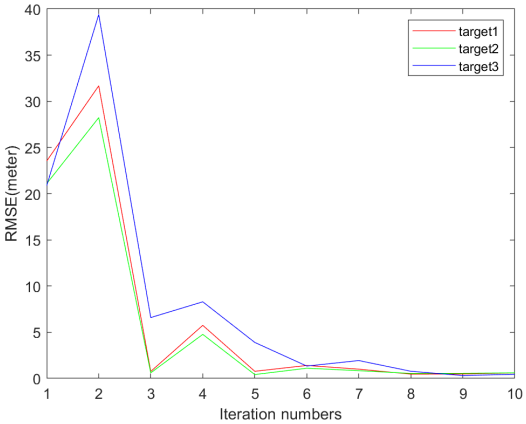

FIGURE 6. Convergence performance of FG-GE in 2D scenario.

TABLE 2. Average RMSE comparison between the proposed and each single schemes.

Average RMSE (meter)			
	Prop.FG-GE	DOA based FG-GE	TOA based FG-GE
target1	0.28	0.87	1.15
target2	0.35	0.86	1.04
target3	0.29	0.88	1.40
	Tracking with Prop.FG-GE	Tracking with DOA based FG-GE	Tracking with TOA based FG-GE
target1	0.79	1.89	2.46
target2	1.73	1.99	5.02
target3	1.92	1.89	3.35

proposed FG-GE-EKF. From the simulation, even though two targets intersect at a point, next state can be accurately estimated, by referring to the previous state. Moreover, to evaluate the accuracy of FG-GE and FG-GE-EKF, the average RMSE with the three algorithms was calculated, of which results are shown in TABLE 2. As shown in the upper half of TABLE 2, in the positioning phase, the proposed FG-GE algorithm can achieve the lowest average RMSE compared to the DOA-only and TOA-only algorithms. In the tracking

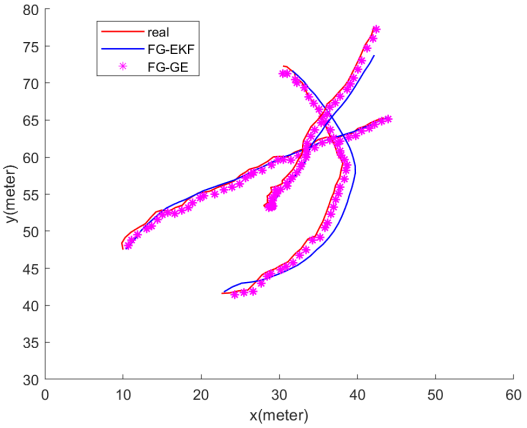

(a) Proposed joint DOA and TOA tracking algorithm

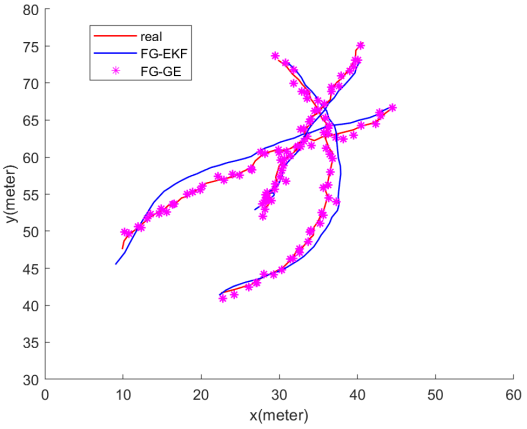

(b) DOA only based tracking algorithm

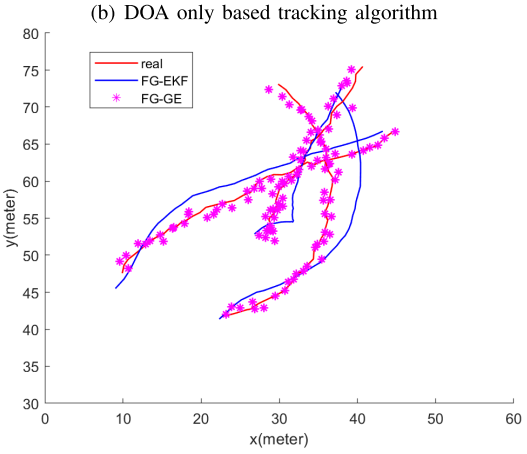

(c) TOA only based tracking algorithm

FIGURE 7. Performance comparison between the proposed and each single schemes.

phase, as shown in the lower half of TABLE 2, the proposed FG-GE-EKF algorithm also achieves the lowest average RMSE among the three algorithms. Finally, the performance accuracy of the proposed FG-GE algorithm is evaluated by comparing the average RMSE with the CRLB. The result is shown in Fig.8. Obviously, the gaps between the average RMSE obtained by the simulations and the CRLBs are very small, especially in the value range of small σ_φ.

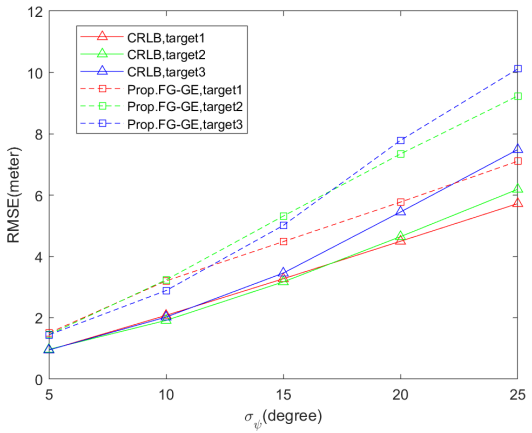

FIGURE 8. Comparison between the average RMSE and the CRLB.

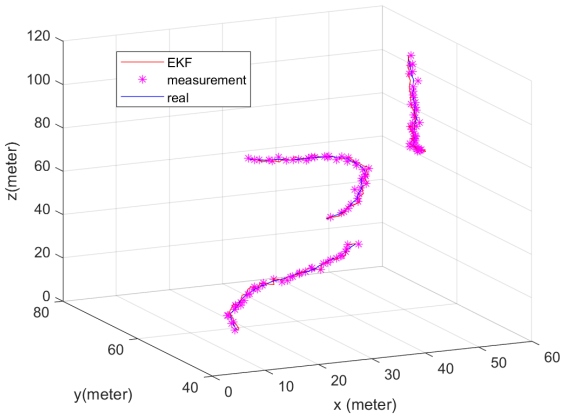

FIGURE 9. tracking trajectories in 3D scenario.

B. 3D SCENARIO

As mentioned before, in the 3D scenario, elevation angle θ is assumed to be obtained from the distributed sensors. The process equations of three targets in the $X-Y$ coordinate are the same as (71)-(76), and only the process equations in the Z coordinate provides additional information. The process equations in the Z coordinate used in the simulation are shown below:

$$z_{1,k} = z_{1,k-1} + \sin\left(\frac{z_{1,k-1}\Phi}{k}\right) + \omega_{z,k}, \tag{77}$$

$$z_{2,k} = z_{2,k-1} + \cos\left(0.2k\Phi\right) + \omega_{z,k}, \tag{78}$$

$$z_{3,k} = z_{3,k-1} + (0.03k - 0.032) + \omega_{z,k}. \tag{79}$$

Since the disadvantageous situations of TOA-only or DOA-only rarely occur in 3D scenario, the FG-GE based on the DOA-only is utilized in the simulation, and the switching algorithm is omitted.

All other parameters are the same as the 2D's case, except that the positions of the distributed sensors and the initial target points were changed: the three distributed sensors were located at (-20, -30, -10), (45, 110, 55) and (100, 30, 60). In 3D geolocation, also three sensors are needed regardless of target numbers. This is because with the proposed technique,

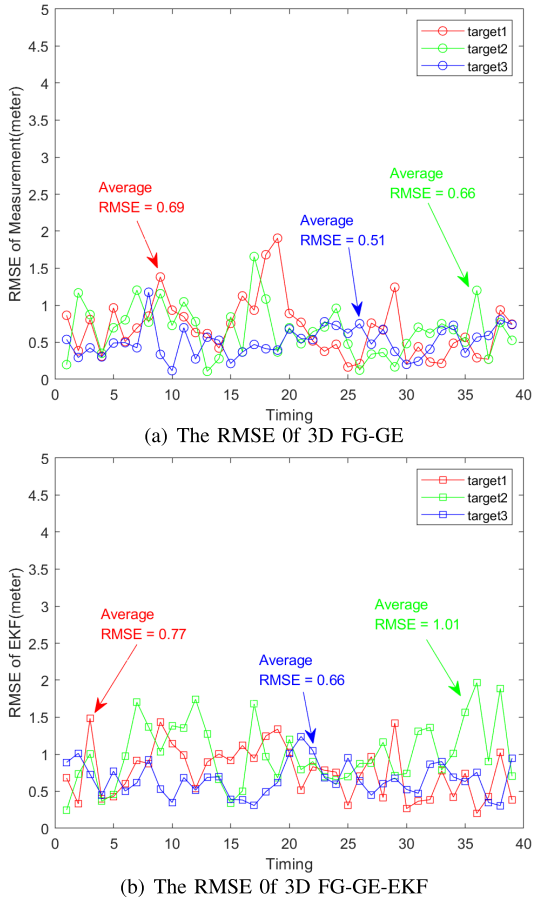

(a) The RMSE 0f 3D FG-GE

(b) The RMSE 0f 3D FG-GE-EKF

FIGURE 10. Performance of position dection and tracking in 3D scenario.

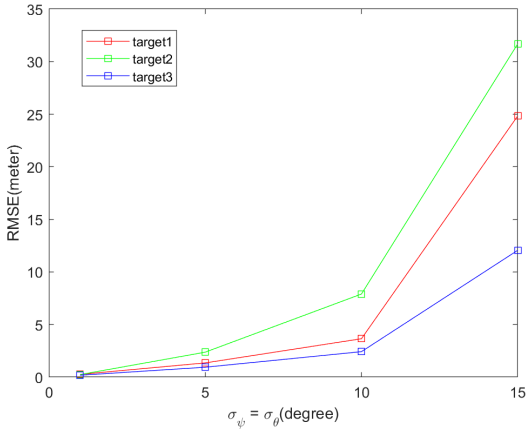

FIGURE 11. Average RMSE versus variance for FG-GE in 3D scenario.

3D geolocation is decomposed into three 2D FG-based geolocations. The initial points of three targets were set at (10, 47.5, 12), (22.6, 41.6, 65) and (48.2, 53.3, 80). We assume that each sensor can obtain 60 samples of azimuth φ and elevation θ, with $\sigma_\varphi = \sigma_\theta = 3°$. By applying the proposed 3D FG-GE and FG-GE-EKF algorithms, the estimated positions of the three targets and the tracking trajectories are shown in Fig.9. It is clearly seen that the estimated positions and tracking trajectories are very close to the real paths in the 3D coordinate.

Then, to evaluate the performance of the position detection and tracking of three targets, the RMSEs of 3D FG-GE and FG-GE-EKF versus timing index are calculated. The results are shown in Fig.10. From the simulation results, the average RMSEs with 3D FG-GE and FG-GE-EKF are very small, which demonstrates excellent performance of the proposed algorithms. Finally, the accuracy of the proposed 3D FG-GE was evaluated by changing σ_φ and σ_θ values. It should be noted that σ_φ and σ_θ may differ among the distributed sensors in practice. However, in the simulation, we assume that the DOA measurements of all sensors have the same standard deviation. Therefore, we set $\sigma_\varphi = \sigma_\theta$. It is found from Fig.11 that the average RMSEs of the three targets are small, especially when σ_φ and σ_θ values are in a small value range.

V. CONCLUSION

This article has proposed a joint multi-target TOA-DOA based geolocation and tracking algorithm both in 2D and 3D scenarios. The combination of TOA and DOA is not only used to compensate for each technique's shortcomings, but also to solve the sensor association problem. According to the simulation results, the proposed joint TOA-DOA algorithm can achieve lower average RMSEs than that with DOA-only and TOA-only techniques. Moreover, the matching problem between the observations and the targets can be solved by the proposed sensor association algorithm in both 2D and 3D scenarios. The performances of the proposed FG-GE technique have been compared with the CRLB. It has been shown that the gaps between the RMSE obtained by the simulation results and the CRLB are very small even though the initial guess points are very far away from the real target positions. For the purpose of target tracking, FG of EKF is further appended to FG-GE, referred to as FG-GE-EKF, which not only can track multi-target in 2D space but also in 3D space. It has been shown that the FG-GE-EKF algorithm can improve the tracking accuracy while reducing computational complexity.

APPENDIX

A. CALCULATION OF THE OBSERVATION NOISE

In this sub-section, the observation noise σ_e^2 is derived for the proposed FG-GE-EKF based on the CRLB derivation. In 2D scenario, σ_e^2 value can be derived from the measured DOA variable φ. Moreover, in 3D scenario, based on the proposed 3D FG-GE algorithm, the target position is projected onto the three planes. The observation noise of each projection point can be similarly derived from the angle information υ and γ. Due to the space limitation, only the derivation of σ_e^2 on $X-Y$ plane is provided. According to [22], the CRLB is given by

$$CRLB = trace[F^{-1}(s)], \tag{80}$$

where F is the Fisher information matrix (FIM). Given the PDF of the variable φ with L samples, the FIM can be derived

by

$$F(s) = E\left[\left(\frac{\partial}{\partial s}\ln p(\widehat{\varphi})\right)^2\right], \tag{81}$$

where the PDF function $p(\cdot)$ is given by

$$p(\widehat{\varphi}) = \prod_{l=1}^{L}\frac{1}{\sqrt{2\pi\sigma_\varphi^2}}\exp\left[-\frac{1}{2\sigma_\varphi^2}(\widehat{\varphi}_l-\varphi)^2\right]. \tag{82}$$

Moreover, (77) can be expressed by

$$E\left[\left(\frac{\partial}{\partial s}\ln p(\widehat{\varphi})\right)^2\right] = -E\left[\frac{\partial^2}{\partial\varphi^2}\ln p(\widehat{\varphi})\right]. \tag{83}$$

According to [19],

$$\frac{\partial^2}{\partial\varphi^2}\ln p(\widehat{\varphi}) = -\frac{L}{\sigma_\varphi^2}. \tag{84}$$

Then, the FIM can further be derived by

$$\begin{aligned} F(s) &= \frac{\partial\varphi}{\partial s}^T E\left[\left(\frac{\partial}{\partial\varphi}\ln p(\widehat{\varphi})\right)^T\left(\frac{\partial}{\partial\varphi}\ln p(\widehat{\varphi})\right)\right]\frac{\partial\varphi}{\partial s} \\ &= \frac{\partial\varphi}{\partial s}^T E\left[\left(\frac{\partial}{\partial\varphi}\ln p(\widehat{\varphi})\right)^2\right]\frac{\partial\varphi}{\partial s} \\ &= \frac{\partial\varphi}{\partial s}^T\left[\frac{L}{\sigma_\varphi^2}\right]\frac{\partial\varphi}{\partial s}. \end{aligned} \tag{85}$$

$\frac{\partial\varphi}{\partial s}$ denotes the Jacobin matrix, which is given by

$$J = \frac{\partial\varphi}{\partial s} = \begin{bmatrix} \frac{\partial\varphi_1}{\partial x} & \frac{\partial\varphi_1}{\partial y} \\ \frac{\partial\varphi_2}{\partial x} & \frac{\partial\varphi_2}{\partial y} \\ \vdots & \vdots \\ \frac{\partial\varphi_N}{\partial x} & \frac{\partial\varphi_N}{\partial y} \end{bmatrix}, \tag{86}$$

with

$$\frac{\partial\varphi_n}{\partial x} = \frac{Y_n - y}{d_n^2}, \tag{87}$$

$$\frac{\partial\varphi_n}{\partial y} = \frac{-(X_n - x)}{d_n^2}, \tag{88}$$

where d_n denotes the Euclidean distance between target and sensor n in $X-Y$ plane and $n = \{1, 2, \cdots, N\}$. In this article, the prediction state $x_{k|k-1}$ and $y_{k|k-1}$ is used at timing k because the real position target (x_k, y_k) is unknown to the system. Therefore, the Jacobin matrix can be expressed by

$$J_{k|k-1} = \begin{bmatrix} \frac{Y_1 - y_{k|k-1}}{d_1^2} & \frac{-(X_1 - x_{k|k-1})}{d_1^2} \\ \frac{Y_2 - y_{k|k-1}}{d_2^2} & \frac{-(X_2 - x_{k|k-1})}{d_2^2} \\ \vdots & \vdots \\ \frac{Y_N - y_{k|k-1}}{d_N^2} & \frac{-(X_N - x_{k|k-1})}{d_N^2} \end{bmatrix}. \tag{89}$$

Finally, the CRLB is derived by

$$CRLB = \{diag[(J_{k|k-1}^T\sum_{\varphi}^{-1}J_{k|k-1})L]\}^{-1}. \tag{90}$$

B. DERIVATION FOR EKF

The objective of EKF is to find the maximum posterior probability $p(s_k, v_k|j_{1:k})$, where subscript $1:k$ is the measurement data series from the timing 1 to k. As in [19], [23], the posterior probability $p(s_k, v_k|j_{1:k})$ can be given by

$$p(s_k, v_k|j_{1:k}) = \sum_{\sim s_k, \sim v_k} p(s_{1:k}, v_{1:k}|j_{1:k}), \tag{91}$$

where $\sim$ denotes the operator of the exclusion. According to Bayes's theorem, the joint distribution (91) can be further expressed as

$$p(s_{1:k}, v_{1:k}|j_{1:k}) = \frac{p(j_k|s_{1:k}, v_{1:k}, j_{1:k-1})p(s_{1:k}, v_{1:k}, j_{1:k-1})}{p(j_{1:k})}. \tag{92}$$

Due to the fact that j_k is only determined by s_k and $p(j_{1:k})$ is constant and hence can be omitted, (92) can be derived as

$$p(s_{1:k}, v_{1:k}|j_{1:k}) \propto p(j_k|s_k)p(s_{1:k}, v_{1:k}, j_{1:k-1}). \tag{93}$$

Further more,

$$\begin{aligned} &p(s_{1:k}, v_{1:k}, j_{1:k-1}) \\ &= p(s_k|s_{k-1}, v_{k-1})p(v_k|v_{k-1})p(s_{1:k-1}, v_{1:k-1}|j_{1:k-1})p(j_{1:k-1}) \\ &\propto p(s_k|s_{k-1}, v_{k-1})p(v_k|v_{k-1})p(s_{1:k-1}, v_{1:k-1}|j_{1:k-1}) \end{aligned} \tag{94}$$

where $j_{1:k-1}$ is ignored hence only s_k is determined by s_{k-1} and v_{k-1}. Further more, v_k is only determined by v_{k-1}. $p(s_{1:k-1}, v_{1:k-1}|j_{1:k-1})$ is recursively related to the state at the previous timing. Therefore, by combining (93) and (94), the posterior probability $p(s_k, v_k|j_{1:k})$ can be derived as follow

$$\begin{aligned} &p(s_{1:k}, v_{1:k}|j_{1:k}) \\ &\propto \prod_{1:k} p(s_k|s_{k-1}, v_{k-1})p(v_k|v_{k-1})p(j_k|s_k). \end{aligned} \tag{95}$$

where $\prod$ represents timing series from 1 to k. According to (95), the EKF process can be divided into 3 parts as follow.

1) STATE PREDICTION

Based on the outputs of FG-GE-EKF at previous timing $k-1$, the prediction message of the next state $s_{k|k-1}$, as shown in Fig.12, can be given by

$$\begin{aligned} &\mu_c(s_{k|k-1}) \\ &= \sum_{s_{k-1}}\sum_{v_{k-1}} f(s_{k|k-1}|s_{k-1}, v_{k-1})\mu_a(s_{k-1})\mu_b(v_{k-1}), \end{aligned} \tag{96}$$

where the messages $\mu_a(s_{k-1})$ and $\mu_b(v_{k-1})$ are from previous state at the timing $k-1$, with the function $f(s_{k|k-1}|s_{k-1}, v_{k-1}) = s_{k-1} + v_{k-1}$.

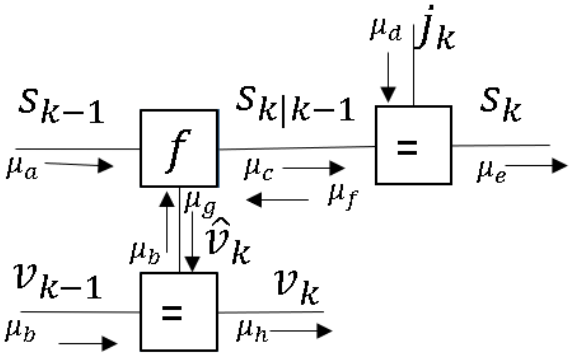

FIGURE 12. Proposed FG-GE-EKF.

2) STATE UPDATE

The current state can be obtained by using the current observation value j_k to refine the state prediction $s_{k|k-1}$, according to the EKF algorithm. Therefore, the current state s_k can be given by

$$\mu_e(s_k) = \mu_c(s_{k|k-1})\mu_d(j_k), \tag{97}$$

where $\mu_d(j_k)$ is the observed value obtained by the proposed position detection FG.

3) GRADIENT UPDATE

Since the gradient vector v_k is only determined by v_{k-1}, we introduce the correction term $\hat{v}_k$ to update v_k. The correction term $\hat{v}_k$ can be obtained by letting two adjacent locations be divided by unit time. Therefore, the message $\hat{v}_k$ is given by

$$\mu_g(\hat{v}_k) = \sum_{s_{k-1}} \sum_{s_k} f(\hat{v}_k|s_{k-1}, s_k)\mu_a(s_{k-1})\mu_f(s_k), \tag{98}$$

where $\mu_f(s_k)$ is the current state message, and the function $f(\hat{v}_k|s_{k-1}, s_k) = s_k - s_{k-1}$. Then, the update of the gradient vector v_k can be obtained by

$$\mu_h(v_k) = \mu_b(v_{k-1})\mu_g(\hat{v}_k). \tag{99}$$

REFERENCES

[1] J. J. Caffery and G. L. Stuber, "Overview of radiolocation in CDMA cellular systems," *IEEE Commun. Mag.*, vol. 36, no. 4, pp. 38–45, Apr. 1998.
[2] S. A. A. Shah, E. Ahmed, M. Imran, and S. Zeadally, "5G for vehicular communications," *IEEE Commun. Mag.*, vol. 56, no. 1, pp. 111–117, Jan. 2018.
[3] I. Aydin, M. Karakose, and E. Karakose, "A navigation and reservation based smart parking platform using genetic optimization for smart cities," in *Proc. 5th Int. Istanbul Smart Grid Cities Congr. Fair (ICSG)*, Apr. 2017, pp. 120–124.
[4] H. Wymeersch, G. Seco-Granados, G. Destino, D. Dardari, and F. Tufvesson, "5G mmWave positioning for vehicular networks," *IEEE Wireless Commun.*, vol. 24, no. 6, pp. 80–86, Dec. 2017.
[5] J. C. Chen, K. Yao, and R. E. Hudson, "Source localization and beamforming," *IEEE Signal Process. Mag.*, vol. 19, no. 2, pp. 30–39, Mar. 2002.
[6] B. E. Caroline, S. C. Xavier, A. P. Kabilan, and J. William, "Performance analysis and comparison of optical signal processing beamforming networks: A survey," *Photonic Netw. Commun.*, vol. 37, no. 1, pp. 38–52, Feb. 2019.
[7] F. Liu, P. Zhao, and Z. Wang, "EKF-based beam tracking for mmwave MIMO systems," *IEEE Commun. Lett.*, vol. 23, no. 12, pp. 2390–2393, Dec. 2019.
[8] R. Mautz, "Overview of current indoor positioning systems," *Geodezija ir Kartografija*, vol. 35, no. 1, pp. 18–22, Jan. 2009.
[9] F. Adib, Z. Kabelac, and D. Katabi, "Multi-person localization via RF body reflections," in *Proc. 12th USENIX Symp. Netw. Syst. Design Implement. (NSDI)*, 2015, pp. 279–292.
[10] T. Farah Sanam and H. Godrich, "CoMuTe: A convolutional neural network based device free multiple target localization using CSI," 2020, *arXiv:2003.05734*. [Online]. Available: http://arxiv.org/abs/2003.05734
[11] F. R. Kschischang, B. J. Frey, and H.-A. Loeliger, "Factor graphs and the sum-product algorithm," *IEEE Trans. Inf. Theory*, vol. 47, no. 2, pp. 498–519, Feb. 2001.
[12] J.-C. Chen, Y.-C. Wang, C.-S. Maa, and J.-T. Chen, "Network-side mobile position location using factor graphs," *IEEE Trans. Wireless Commun.*, vol. 5, no. 10, pp. 2696–2704, Oct. 2006.
[13] W. Foy, "Position-location solutions by Taylor-series estimation," *IEEE Trans. Aerosp. Electron. Syst.*, vol. AES-12, no. 2, pp. 187–194, Mar. 1976.
[14] J.-C. Chen, P. Ting, C.-S. Maa, and J.-T. Chen, "Wireless geolocation with TOA/AOA measurements using factor graph and sum-product algorithm," in *Proc. IEEE 60th Veh. Technol. Conf. (VTC-Fall)*, Sep. 2004, pp. 3526–3529.
[15] H.-L. Jhi, J.-C. Chen, C.-H. Lin, and C.-T. Huang, "A factor-graph-based TOA location estimator," *IEEE Trans. Wireless Commun.*, vol. 11, no. 5, pp. 1764–1773, May 2012.
[16] C. Mensing and S. Plass, "TDOA positioning based on factor graphs," in *Proc. IEEE 17th Int. Symp. Pers., Indoor Mobile Radio Commun.*, Sep. 2006, pp. 1–5.
[17] C.-T. Huang, C.-H. Wu, Y.-N. Lee, and J.-T. Chen, "A novel indoor RSS-based position location algorithm using factor graphs," *IEEE Trans. Wireless Commun.*, vol. 8, no. 6, pp. 3050–3058, Jun. 2009.
[18] S. N. Karimah, M. R. K. Aziz, and T. Matsumoto, "A hybrid TOA and RSS-based factor graph for wireless geolocation technique," in *Proc. IEEE 12th Int. Colloq. Signal Process. Its Appl. (CSPA)*, Mar. 2016, pp. 140–145.
[19] M. Cheng, M. R. K. Aziz, and T. Matsumoto, "Integrated factor graph algorithm for DOA-based geolocation and tracking," *IEEE Access*, vol. 8, pp. 49989–49998, Mar. 2020.
[20] Z. Lin, Q. Zou, E. S. Ward, and R. J. Ober, "Cramer-rao lower bound for parameter estimation in nonlinear systems," *IEEE Signal Process. Lett.*, vol. 12, no. 12, pp. 855–858, Dec. 2005.
[21] M. Cheng, M. R. K. Aziz, and T. Matsumoto, "A DOA-based factor graph technique for 3D multi-target geolocation," *IEEE Access*, vol. 7, pp. 94630–94641, Jul. 2019.
[22] M. R. Kahar Aziz, K. Anwar, and T. Matsumoto, "A new DOA-based factor graph geolocation technique for detection of unknown radio wave emitter position using the first-order Taylor series approximation," *EURASIP J. Wireless Commun. Netw.*, vol. 2016, no. 1, p. 189, Aug. 2016.
[23] H. Wymeersch, *Iterative Receiver Design*, vol. 234. Cambridge, U.K.: Cambridge Univ. Press, Sep. 2007.

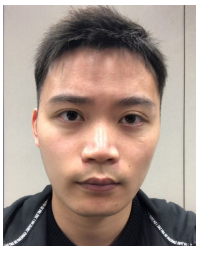

LEI JIANG received the B.S. degree in electronic and information engineering from the University of Science and Technology at Liaoning, Liaoning, China, in 2017. He is currently pursuing the M.S. degree with the Japan Advanced Institute of Science and Technology, Ishikawa, Japan. His research interests include network information theory, iterative coding/decoding, and wireless geolocation techniques.

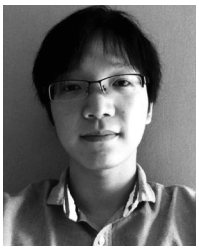

MENG CHENG (Member, IEEE) received the B.Eng. degree in telecommunication engineering from the Anhui University of Technology, Anhui, China, in 2009, the M.Sc. degree (Hons.) in wireless communications from the University of Southampton, Southampton, U.K., in 2010, and the Ph.D. degree in information science from the Japan Advanced Institute of Science and Technology (JAIST), Ishikawa, Japan, in 2014. He has served as a 5G Research Engineer with the Shanghai Research Center, Huawei Technologies Company, Ltd., from 2014 to 2017. After that, he returned to JAIST as a Postdoctoral Researcher. His research interests are network information theory, non-orthogonal multiple access, iterative coding/decoding, and wireless geolocation techniques.

TAD MATSUMOTO (Life Fellow, IEEE) received the B.S. and M.S. degrees in electrical engineering under the supervision of Prof. S.-I. Takahashi, and the Ph.D. degree in electrical engineering under the supervision of Prof. M. Nakagawa from Keio University, Yokohama, Japan, in 1978, 1980, and 1991, respectively. In 1980, he joined Nippon Telegraph and Telephone Corporation (NTT), where he was involved in a lot of research and development projects, all for mobile wireless communications systems. In 1992, he transferred to NTT DoCoMo, where he researched on code-division multiple-access techniques for mobile communication systems. In 1994, he transferred to NTT America, where he served as a Senior Technical Advisor of a joint project between NTT and NEXTEL Communications. From 1996 to 2001, he returned to NTT DoCoMo, where he served as the Head of the Radio Signal Processing Laboratory. He researched on adaptive signal processing, multiple-input multiple-output turbo signal detection, interference cancellation, and space-time coding techniques for broadband mobile communications. In 2002, he moved to the University of Oulu, Finland, where he served as a Professor with the Centre for Wireless Communications. In 2006, he served as a Visiting Professor with the Ilmenau University of Technology, Ilmenau, Germany, supported by the German MERCATOR Visiting Professorship Program. Since 2007, he has been serving as a Professor with the Japan Advanced Institute of Science and Technology, Japan, and also a cross-appointment position with the University of Oulu. He has led a lot of projects funded by the Academy-of-Finland, European FP7, and the Japan Society for the Promotion of Science and by Japanese private companies. He was appointed as a Finland Distinguished Professor from 2008 to 2012, supported by the Finnish National Technology Agency (Tekes) and the Finnish Academy, under which he preserves the rights to participate in and apply to European and Finnish national projects. He is a member of the IEICE. He was a recipient of the IEEE VTS Outstanding Service Award in 2001, the Nokia Foundation Visiting Fellow Scholarship Award in 2002, the IEEE Japan Council Award for Distinguished Service to the Society in 2006, the IEEE Vehicular Technology Society James R. Evans Avant Garde Award in 2006, the Thuringen State Research Award for Advanced Applied Science in 2006, the 2007 Best Paper Award of Institute of Electrical, Communication, and Information Engineers of Japan in 2008, the Telecom System Technology Award by the Telecommunications Advancement Foundation in 2009, the IEEE COMMUNICATION LETTERS Exemplary Reviewer in 2011, the Nikkei Wireless Japan Award in 2013, the IEEE VTS Recognition for Outstanding Distinguished Lecturer in 2016, and the IEEE TRANSACTIONS ON COMMUNICATIONS Exemplary Reviewer in 2018. He has been serving as an IEEE Vehicular Technology Distinguished Speaker, since 2016.